

Polarized microphotoluminescence and reflectance spectroscopy of GaN with \mathbf{k} perpendicular to \mathbf{c} : Strongly π -polarized line near the A exciton

T. V. Shubina,¹ T. Paskova,² A. A. Toropov,¹ S. V. Ivanov,¹ and B. Monemar²

¹*Ioffe Institute of RAS, Politekhnicheskaya 26, 194021 St. Petersburg, Russia*

²*Linköping University, S-581 83 Linköping, Sweden*

(Received 23 April 2001; revised manuscript received 4 September 2001; published 1 February 2002)

Polarized microphotoluminescence (μ -PL) and reflectivity studies of thick wurtzite GaN grown by hydride vapor phase epitaxy on c sapphire are performed with the light vector \mathbf{k} both normal to the \mathbf{c} axis ($\mathbf{k}\perp\mathbf{c}$) and parallel to it. A strong PL peak is found in the vicinity of the A exciton in π polarization ($\mathbf{k}\perp\mathbf{c}$, \mathbf{E} parallel to the \mathbf{c} axis), in apparent contradiction to the selection rules. The π -polarized component exceeds in intensity the σ -polarized one up to ~ 50 K. Power- and temperature-dependent measurements of both no-phonon and longitudinal optical phonon-assisted (monitoring the real density of exciton states) μ -PL reveal the complex nature of the π -polarized PL line near the A exciton. At low temperatures the π -component involves a bound B exciton contribution, while at higher temperatures contributions of scattered A exciton states become appreciable. The enhancement of the π -polarized component is attributed to the complex structure of the exciton-polariton branches for $\mathbf{k}\perp\mathbf{c}$. Temperature-dependent μ -PL and reflectance spectroscopies reveal additionally a difference in the optical properties between the sample regions at the top surface and the cleaved edges, tentatively explained as induced by different strains in these regions.

DOI: 10.1103/PhysRevB.65.075212

PACS number(s): 71.35.Cc, 71.36.+c, 78.55.Cr, 78.66.Fd

I. INTRODUCTION

The generally accepted picture of the valence band physics of GaN is based on the experimental study of optical reflectance (R) by Dingle *et al.* made in 1971.¹ Besides the conventionally performed measurements at α -polarization, when the light wave vector \mathbf{k} is parallel to the principal axis \mathbf{c} , and the electric field vector \mathbf{E} is normal to it, these authors registered spectra in π - ($\mathbf{k}\perp\mathbf{c}, \mathbf{E}\parallel\mathbf{c}$) and σ - ($\mathbf{k}\perp\mathbf{c}, \mathbf{E}\perp\mathbf{c}$) polarizations. That permitted one, for the first time, to directly establish the ordering of the valence bands in GaN, to check selection rules, and to determine the crystal-field splitting and the spin-orbit interaction parameters by using Hopfield's quasicubic model.² However, the study of optical properties of GaN with $\mathbf{k}\perp\mathbf{c}$ cannot be considered as complete. Polarized photoluminescence (PL) spectra were not presented by Dingle *et al.*, but they pointed out differences between the α - and σ -polarized reflectance spectra, which should not be present in the classical model. To the best of our knowledge, these experiments have not been repeated so far, due to obvious difficulties in preparing perfect facets parallel to the \mathbf{c} axis. As a result, correspondence of PL and R spectra of GaN is established reliably only for the α polarization. There are also very few papers³⁻⁷ concerning the $\mathbf{k}\perp\mathbf{c}$ luminescence properties, although such data are rather important for GaN-based LED and laser performance, because in these devices light propagates along the epitaxial layers.

Temperature-dependence studies of PL properties are widely used to assign excitonic transitions in GaN, particularly to exclude a misinterpretation between free (FX) and bound (BX) excitonic states.⁸ As was shown by Gil, Briot, and Aulombard the energy of the excitonic transitions is controlled by the internal strain⁹ which, in general, depends on the temperature, the size of GaN columns, as well as on types and density of dislocations in the epitaxial layers.

The conventional PL and R measurements tend to smooth out inherent peculiarities of excitonic spectra, averaging parameters among the perfect and defective regions. For a proper study of GaN optical properties, the μ -PL technique with high spatial resolution is much more informative. It is worth noting that different spatially resolved optical techniques (μ -PL, cathodoluminescence, near-field scanning optical microscopy) were previously used to study various properties such as the strain distribution across the layers and the PL efficiency in a quantum well or in the vicinity of defects.^{4,7,10-13}

Recently, we have demonstrated the possibility to measure μ -PL and R in different linear polarizations from a facet of thick GaN (0001) epilayers grown by hydride vapor phase epitaxy (HVPE).¹⁴ The unexpected dominance of a π -polarized line [marked below as $X(\pi)$] in the vicinity of the σ -polarized A exciton [$FX_A(\sigma)$] was observed *inter alia* in low-temperature spectra, which obviously contradicts the selection rules for optical transitions in the wurtzite crystal.

As can be seen in Fig. 1(a), the intensity of $X(\pi)$ line is almost twice that of $FX_A(\sigma)$. Since the line coexists with a pure π -polarized free B exciton line [$FX_B(\pi)$] in the spectra, the observation is realistic. To elucidate the origin of the dramatic effect we performed detailed power- and temperature-dependent μ -PL [both no-phonon and longitudinal optical (LO) phonon-assisted emission] and temperature-dependent R studies at different polarizations.

In the paper we present: (i) evidences favoring the notion that $X(\pi)$ mostly originates from internal regions of GaN layers; (ii) an accurate attribution and analysis of the μ -PL and R features; (iii) data on temperature-dependent variation of the real density of differently polarized excitonic states, obtained from analysis of the LO phonon-assisted emission. More than 3-decades-old data on facet reflectance are reexamined using the microscopy measurements at different tem-

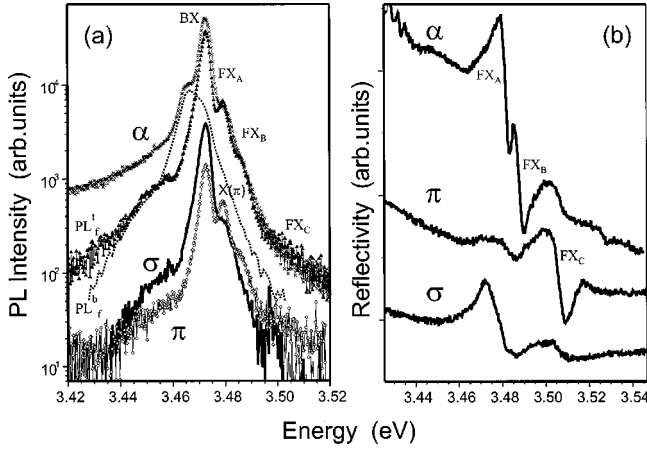


FIG. 1. (a) μ -photoluminescence spectra measured at 5 K in a GaN layer grown on an undoped buffer in different polarizations: α ($\mathbf{k} \parallel \mathbf{c}, \mathbf{E} \perp \mathbf{c}$)—crosses; σ ($\mathbf{k} \perp \mathbf{c}, \mathbf{E} \perp \mathbf{c}$)—solid line; π ($\mathbf{k} \perp \mathbf{c}, \mathbf{E} \parallel \mathbf{c}$)—diamonds. Nonpolarized PL spectra from a facet are also shown by triangles and the dotted curve for the top (PL_f^t) and lower (PL_f^b) regions, respectively. (b) Polarized reflectance spectra taken in the same points where the polarized μ -PL spectra were measured.

peratures, which reliably demonstrate the nonequivalence of regions close to the cleaved edges and the internal regions in GaN epitaxial layers. The work is organized as follows. A brief description of exciton-polaritons in GaN (Sec. II), as well as of the experimental details with some peculiarities of the μ -PL measurements (Sec. III) precedes the presentation of the experimental results obtained in different polarizations at different excitation powers and temperatures (Sec. IV). In Sec. V, we discuss possible mechanisms of the enhancement of the π -polarized line.

II. EXCITON-POLARITONS IN GaN

Free exciton transitions A , B , and C in GaN, like in any other hexagonal crystal with C_{6v} point group symmetry, originate from crystal-field and spin-orbit splitting. The basic excitonic states are the fourfold degenerated $A(\Gamma_7 \times \Gamma_9)$, $B(\Gamma_7 \times \Gamma_7)$, and $C(\Gamma_7 \times \Gamma_7)$ exciton series. The exchange interaction removes the degeneracy and splits the A ($n=1$) level into an allowed Γ_5 state with the angular projection $M = \pm 1$ and a forbidden Γ_6 with $M = \pm 2$. Both ground B and C excitons split into three levels: Γ_5 ($M = \pm 1$), Γ_1 ($M = 0$), and Γ_2 ($M = 0$). The allowed optical transitions involve the Γ_1 state in the $\mathbf{E} \parallel \mathbf{c}$ polarization and the Γ_5 state for $\mathbf{E} \perp \mathbf{c}$.¹⁵ Light with $\mathbf{E} \perp \mathbf{k}$, propagating either along or normal to the c axis, will excite different excitonic transitions. If $\mathbf{k} \parallel \mathbf{c}$, i.e., $\mathbf{E} \perp \mathbf{c}$, then three α -polarized Γ_5 levels of A , B , and C excitons can be observed, while at $\mathbf{k} \perp \mathbf{c}$ there are either the same three σ -polarized Γ_5 levels (if $\mathbf{E} \perp \mathbf{c}$) or two π -polarized Γ_1 levels of the B and C excitons (if $\mathbf{E} \parallel \mathbf{c}$). The oscillator strengths of $C(\Gamma_1)$ and $A(\Gamma_5)$ are strongest, while moderate strengths are expected for $B(\Gamma_5)$ and $B(\Gamma_1)$, and a small one for $C(\Gamma_5)$.¹

To describe accurately the performance of excitons in high-quality GaN, one should take into account the polariton concept, which considers coupling between photons and free

excitons.¹⁶ Generally, this coupling is strong in direct-band-gap polar semiconductors with dipole-active excitons, to which GaN belongs, and means a continual energy exchange between the photon electric field and free excitons through polarizability. This results in a spatial dispersion of the dielectric function $\epsilon(\mathbf{k}, \omega)$. In this case a two-branch dispersion curve in \mathbf{k} space, consisting of an upper polariton branch (UPB) and a lower polariton branch (LPB), is expected for each excitonic state. Thus, polaritons influence characteristic energies and shapes of peculiarities in optical spectra and cause specific effects related to different curvature of the branches. It is important that polariton fluorescence occurs on the surface, while wave packets can form deep inside a crystal.¹⁷

Currently, it is implied that exciton-polaritons exist in GaN if there are well-resolved free-exciton features in reflectance spectra.¹⁸ Obviously, any factor causing either “death” of a free exciton or accidental variation of its properties, such as strain or electric field fluctuations near defects, inhibits the polariton formation. The same structural imperfections induce the experimentally observed inhomogeneous broadening of exciton resonances in high-quality GaN. Therefore one can assume that polaritons may be maintained in a GaN crystal if the PL linewidth is comparable with the longitudinal-transverse splitting Δ_{LT} , which is a measure of the light-exciton interaction. In high-quality GaN grown by homoepitaxy^{18,19} or lateral epitaxial overgrowth^{20,21} the observation of distinct polariton features is consistent with this empirical rule, and directly reflects the low density of defects. In thick GaN layer, e.g., grown by HVPE on sapphire, the average density of defects is higher, but it drops significantly towards the top surface.^{22,23} The free excitons can easily survive there providing the mixed states. The polariton formation is facilitated for the light spreading along the top perfect layer region with $\mathbf{k} \perp \mathbf{c}$.

The electron-hole pairs (or excitons) created nonresonantly in the continuum states relax towards lower energy of the two branches using phonon-^{24,25} or impurity-assisted²⁶ scattering and then convert into photons at the surface. During the scattering processes the polariton states can be captured by different radiative and nonradiative states and lose their polarization. At normal registration the spectral efficiency of the polariton PL is given as²⁷

$$I(E) \cong \sum_r T_r(E) v_r(E) F_r(x, E) \rho_r(E) \Delta E, \quad (1)$$

where $T_r(E)$ is the transmission coefficient of the r polariton branch at the crystal boundary; $F_r(x, E)$ is the distribution function of the polariton branches at a point x ; $\rho_r(E)$ is the density of polariton states. The process depends strongly on the polariton group velocity $v_p = \hbar^{-1} dE/dk$, where E and k are the energy and wave vector of the polariton, respectively. An increase of the polariton population at low v_p results in the appearance of the so-called bottleneck spectral region.²⁸

The polariton emission frequently has a doublet shape with the energy gap between the components close to Δ_{LT} .²⁹ The doublet has been attributed to luminescence from the

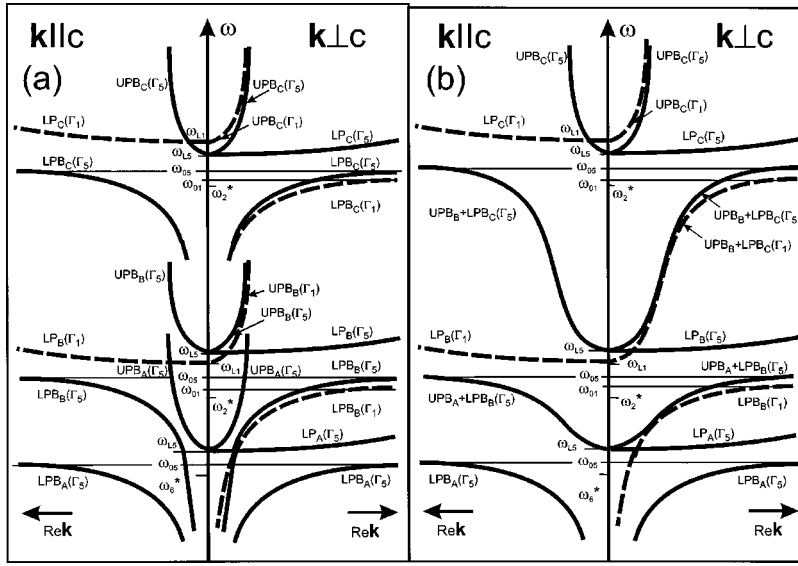


FIG. 2. Energy diagrams of separate (a) and integrated (b) polaritons in GaN. The left panel of each diagram shows polariton branches for $\mathbf{k}\parallel\mathbf{c}$, right—for $\mathbf{k}\perp\mathbf{c}$. Solid and dashed curves denote polaritons with possible emission in σ - and π -polarizations, respectively; LP is a longitudinal polariton, UPB and LPB are upper and lower polariton branches, respectively; ω_i denotes characteristic energies of the exciton-polariton branches.

LPB and UPB, with reabsorption and elastic scattering of polaritons, e.g., by neutral impurities. Recent studies assigned such a doublet in GaN to emission from the LPB and UPB,^{18,20,30} though the connection with the residual donor concentration was also demonstrated.¹⁸

Besides the no-phonon emission, additional PL bands can be observed in the GaN samples, separated approximately by LO phonon energy of ~ 92 meV. The LO phonon-assisted PL occurs in the region of transparency, where the group velocity is high, and can be used to analyze a real density of exciton-polariton states.¹⁷ In the thermal equilibrium with the crystal lattice the m th phonon band has intensity described by the Maxwell-like distribution

$$I_m^{\text{LO}} \sim [dN(k)/N] W_m(k) \sim E^{1/2} \exp(-E/k_B T) W_m(E), \quad (2)$$

where E is the kinetic energy of the exciton, N is the density of the polariton states, $W_m(k, E)$ is the energy-dependent probability of exciton recombination with an emission of m LO phonons.³¹

Since the polariton branches originate from the appropriate excitonic transitions, the light propagation along or normal to the \mathbf{c} axis, respectively, provides different sets of polaritons as shown schematically in Fig. 2(a), where transitions allowed for $\mathbf{E}\perp\mathbf{c}$ and $\mathbf{E}\parallel\mathbf{c}$ are shown by solid and dashed curves, respectively. The scheme is composed using data published for polaritons in II-VI wurtzite compounds.³² The mutual positions of the polariton branches related to the Γ_5 and Γ_1 exciton states, depending on a strain in the structure, need a closer study. Here we demonstrate the expected structure of these branches by using available theoretical estimates.³³ The energy positions of forbidden transitions frequently observed in polariton emission in different materials^{16,24,34} are marked (by stars) tentatively due to the lack and dispersion of respective data for GaN.^{5,6} One can see that the transverse UPB and longitudinal polaritons (LP) are connected pairwise for $\mathbf{k}\parallel\mathbf{c}$ and $\mathbf{k}\perp\mathbf{c}$ for both excitons Γ_5 and Γ_1 . It is worth noting that the longitudinal polaritons in

GaN are usually not taken into account because of stronger coupling of excitons with light in the transverse polariton modes.

The pattern of polariton branches at $\mathbf{k}\perp\mathbf{c}$ is obviously more complicated than that for $\mathbf{k}\parallel\mathbf{c}$. Moreover, there are differently polarized polaritons that coexist at the same energy and sufficiently close \mathbf{k} values. For instance, for $\mathbf{k}\parallel\mathbf{c}$ in the vicinity of the A exciton ground state there is only an α -polarized, photonlike branch of $\text{LPB}_B(\Gamma_5)$, while for $\mathbf{k}\perp\mathbf{c}$, in addition to the σ -polarized $\text{LPB}_B(\Gamma_5)$, there are a π -polarized $\text{LPB}_B(\Gamma_1)$ and a σ -polarized longitudinal polariton originating from the Γ_5 exciton state.

The GaN has a significant dissimilarity to the II-VI semiconductors, such as CdS, CdSe, etc.—smaller energy gaps between the three top valence bands, which results in an appreciable overlap of polariton branches originating from different excitonic states. Generally, the overlapping polaritons should be considered together as a combined branch. For $\mathbf{k}\parallel\mathbf{c}$ the interaction of the UPB related to the A band with the LPB of the B band was first demonstrated in Ref. 30. Four transverse polariton branches, $\text{LPB}_A(\Gamma_5)$, $\text{UPB}_A + \text{LPB}_B(\Gamma_5)$, $\text{UPB}_B + \text{LPB}_C(\Gamma_5)$, and $\text{UPB}_C(\Gamma_5)$ have been determined in GaN by solving the coupled exciton-polariton dispersion equations^{18,20} (here the sign “+” denotes integration over the respective branches). The branches combining for $\mathbf{k}\parallel\mathbf{c}$, all originating from Γ_5 , are shown in Fig. 2(b), left panel. We believe that the same phenomenon has to take place for $\mathbf{k}\perp\mathbf{c}$. The integration should involve the excitonic states with similar orientation of the electric dipoles. Thus, the total number of branches increases up to seven at $\mathbf{k}\perp\mathbf{c}$: four Γ_5 branches described above and three additional originating from Γ_1 excitonic states: $\text{LPB}_B(\Gamma_1)$, $\text{UPB}_B + \text{LPB}_C(\Gamma_1)$, and $\text{UPB}_C(\Gamma_1)$ [see Fig. 2(b), right panel].

III. EXPERIMENTS

A. Experimental details

The study was performed using two representative samples with the same thickness of about 25 μm , grown on

c-plane sapphire by using undoped or Si-doped 2.5- μm -thick metal-organic chemical vapor deposited (MOCVD) GaN templates. The growth of the samples was performed at 1090 °C in a conventional HVPE system, as described previously.²³ The samples were nominally undoped, but showed *n*-type conductivity. The level of residual donor concentration determined from Hall measurements in the sample grown on the Si-doped template (2×10^{17} to $4 \times 10^{17} \text{ cm}^{-3}$) is a few times higher than that in the sample grown on the undoped template.²³ The optical study follows a detailed structural characterization by x-ray diffractometry (XRD) and transmission electron microscopy,^{23,35} which demonstrate a good quality of the samples, especially in the vicinity of the top surface region, where the dislocation density is less than 10^8 cm^{-2} . At room temperature the layers exhibit a biaxial compressive strain $\sim 0.2 \text{ GPa}$ at the top surface. Both samples show identical PL spectra from the top surface with very similar energy positions of the PL peaks. Here we present mostly the data obtained on the sample grown on the undoped buffer, since it can be considered as a single crystal with a record small value of column tilt ($\sim 62 \text{ arcsec}$).³⁵ Thus, the sample is expected to possess a minimal value of depolarization due to the *c*-axis inclination.

Measurements of $\mu\text{-PL}$ were carried out in a He continuous flow cryostat in the 4–300 K temperature range under cw excitation by a 266-nm laser line. The UV radiation is emitted by a solid-state diode-pumped frequency-doubled Nd:vanadate cw laser followed by an MDB-266 frequency-doubler unit. The maximal excitation power before the cryostat window was $\sim 12 \text{ mW}$. The beam impinging normally onto a surface or a cleaved edge facet of the sample was focused using a reflective objective creating an excitation spot with full width at half maximum (FWHM) of $\sim 1.5 \mu\text{m}$. The same objective collected the PL signal and the sample image, which is monitored by a charge-coupled detector (CCD). The PL was relayed to the slits of an asymmetrical Czerny-Turner-type monochromator and then to the nitrogen cooled CCD. The maximal spectral resolution of the system is estimated as $\sim 0.6 \text{ meV}$. The $\mu\text{-R}$ measurements were performed in the same setup, using a tungsten lamp as an excitation source. At the same focusing conditions the spatial resolution of the reflectance measurements is estimated as about $10 \mu\text{m}$. A linear polarizer (followed by a depolarizer) is mounted before the monochromator slits to analyze the $\mu\text{-PL}$ and *R*. Two positions of the polarizer were exploited with polarization vectors normal and parallel to the growth direction of the layers (*c* axis), respectively. The samples were characterized by conventional PL and *R* spectra, measured in a closed-cycle He cryostat using a 325 nm line of a 15 mW He-Cd laser and emission of a xenon lamp, respectively, as excitation sources. A photomultiplier with a photon-counting system was used during these experiments. All spectra were calibrated with emission lines of a mercury lamp. The reflectance spectra were normalized using scans obtained from a polished aluminum mirror. During the micro-PL measurements special measures (marking) were taken to maintain the focusing on the same point.

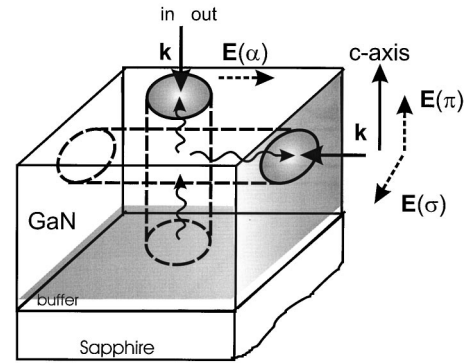


FIG. 3. Scheme of the top surface and facet measurements in different polarizations.

B. Peculiarities of $\mu\text{-PL}$ measurements

Some peculiarities of facet and top surface measurements have to be discussed before analysis of experimental data. As is well known, heteroepitaxial GaN layers have a mosaic structure consisting of columns. In the samples studied the column sizes are in the range of 0.6–1 μm .³⁵ Reflectance spectroscopy, being a surface-sensitive technique, probes especially the outermost first array of such columns. The strain and the defect density differ in the top surface layer and the cleaved edge faces, thus the respective *R* spectra must be unequal. Contrary to that, $\mu\text{-PL}$ spectroscopy is designed to probe the internal part of the layers and the spectra could be similar.

Another peculiarity may be induced by the geometry of the $\mu\text{-PL}$ measurements, when different sections of the GaN layers are excited (Fig. 3). When the excitation is normal to the top surface, the emission from the top layer may be absorbed by underlying more defective or relaxed (adjusted to the buffer) regions and then reemitted with the energy below the top layer absorption edge (in the range of transparency). At the edge $\mu\text{-PL}$ measurements the light of excitation, first coming onto the outmost facet region, penetrates through a relatively uniform longitudinal section (e.g., in the perfect top region). The cleaved edge region is most likely defective and relaxed, and therefore possesses lower transition energy as compared with the internal region. Its emission, which is expected to be weak, cannot be an efficient source for excitation of the rest material.

A high density of excitation, characteristic of the $\mu\text{-PL}$, is a critical factor for observation of exciton-polariton effects, which, as mentioned above, are pronounced if the spectral linewidth is close to the longitudinal-transverse splitting, whose reported values for GaN vary in the $\sim 1\text{--}2 \text{ meV}$ range.^{18,36} In high-quality GaN samples the width of polariton reflection anomalies is close to Δ_{LT} , while the exciton-polariton emission peaks are usually wider (1.5–2.5 meV).^{18,20,21,36} One could expect that the $\mu\text{-PL}$ technique, focusing on the perfect regions, could provide narrower peaks, however, the high density of excitation must result in an increase of population of the polariton branches and, hence, in broadening the PL lines. In our samples the width of peaks rises almost twice with variation of the excitation power in the available range ($\sim 5\text{--}500 \text{ kW cm}^{-2}$). That

makes problematic the observation of pure polariton effects related, for instance, to the splitting between UPB and LPB.

At the same time, as was shown previously,^{38,39} an increase in the photoexcitation density enhances the exciton lifetime, since the different centers, capturing excitons, are saturated and, hence, the exciton-polariton diffusion length increases. We estimate the variation of the effective diffusion length with power by using the integral intensity of 2LO emission, which reflects directly the population of the exciton-polaritons in the whole occupied volume. It has been found that in the μ -PL the rise of the 2LO-line intensity is superlinear, i.e., doubling of the power results in almost five times increase of the 2LO-replica intensity. Thus, the diffusion length at the μ -PL is hardly less than $5 \mu\text{m}$, if we assume that it is $\sim 1\text{--}2 \mu\text{m}$ at the conventional PL. This makes credible the observation of some polariton effects, e.g., related to complicated structure of polariton branches at $\mathbf{k}\perp\mathbf{c}$.

IV. RESULTS AND ANALYSIS

A. Assignment of peaks by using μ -PL and reflectance data

The comparison of μ -PL and R data presented in Fig. 1 permits us to assign the most intense peak to a donor-bound A exciton that appears to be generally σ polarized. The ordering and energy of the free excitonic transitions are consistent with published data for weakly strained GaN on sapphire (see, e.g., references in Ref. 40). The width of the polarized components depends on excitation power: according to a decomposition of the PL band by using Lorentzian contours, an average value is about 3 meV. As for free exciton PL lines, this is slightly more than in strain-free homoepitaxial GaN films,^{18,20,37} as expected. The width of the bound exciton lines is also larger than the best reported values [~ 0.1 meV (Refs. 37,41)] and fine structure of bound excitonic states is not resolved due to the high level of the μ -PL excitation. However, the samples studied are characterized by the distinct excitonic features in the spectra, and the ratio of bound-to-free exciton intensities of about 5:1, which is typical of good quality structures with a residual donor concentration in the low 10^{17} cm^{-3} range.¹⁸

The above-discussed differences between surface and facet measurements are confirmed by the experimental data. The μ -PL spectra recorded in three polarizations from the surface (α) and facet (σ and π) (Fig. 3) are shown in Fig. 1(a) together with the unpolarized facet PL taken from the bottom interface and top regions (PL_f^b and PL_f^t , respectively). The facet PL varies across the layer due to different strain and dislocation densities.¹⁴ The longitudinal homogeneity of the sample body in the top region is, likely, responsible for the distinctiveness of the free exciton features in the facet spectra as compared with the surface one. A differential feature in the α -polarized μ -PL spectrum—the pronounced low-energy shoulder—obviously repeats the PL_f^b [dotted curve in Fig. 1(a)], and is related to remission from bottom interface regions.

The reflectance spectra [Fig. 1(b)] generally satisfy the selection rules and the expected intensity relationship of the exciton transitions. For the α - and σ -polarizations the

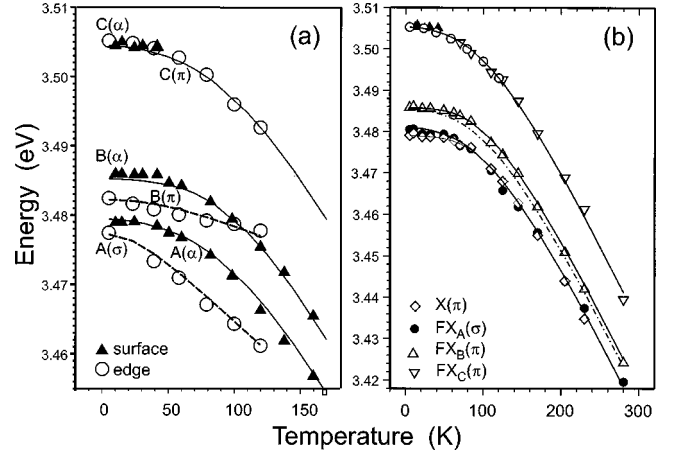


FIG. 4. Temperature dependencies of exciton energies obtained from polarized reflectance (a) and μ -photoluminescence together with reflectance data on the C exciton (b). Open circles and solid triangles show edge and surface reflectance data, respectively. The solid and dashed lines present, respectively, fits to the experimental μ -PL and reflectance points using the Pässler formula; the dash-dotted line presents the fit of $FX_B(\pi)$ with adjusting parameters like for $FX_A(\sigma)$.

$FX_A(\Gamma_5)$ and $FX_B(\Gamma_5)$ exciton resonances are well pronounced, while the $FX_C(\Gamma_5)$ one is rather weak. On the contrary, in the π polarization, the $FX_C(\Gamma_1)$ resonance dominates with a well-distinguished $FX_B(\Gamma_1)$ feature and negligible $FX_A(\Gamma_5)$. According to the fitting of the α -polarized reflectance spectra, using a three oscillators model of the dielectric function,⁴² the linewidth Γ_x is ~ 4 meV. This value is ~ 3 times worse than that for the high-quality epitaxial layer.¹⁸ The R exciton resonances are smoother in the facet spectra, likely due to the cleaved edge imperfection.

The α - and σ -polarized R spectra are unequal—the α -polarized spectrum is high-energy shifted as compared to the σ -polarized one. The difference between the α - and σ -polarized R spectra becomes more dramatic with the temperature variation [Fig. 4(a)]. The exciton resonances, attributed to the same band, shift differently in the facet and surface spectra, although the energy gap between the Γ_5 and Γ_1 states is expected to be less than 2 meV.³⁶ The facet R dependences look as if they were induced by a strong anisotropic strain in this region.⁴³

The detailed analysis of the reflectivity data will be presented elsewhere. Here we would like to stress that the temperature variations of the A and B exciton peak energies obtained from μ -PL measurements [the solid lines in Fig. 4(a)] are consistent with those in the α -polarized R spectrum, but do not correlate with the facet ones. Only the C exciton transitions, energy shifted due to the spin-orbit splitting, show a consistent temperature variation in all spectra. The equal behavior of the μ -PL and the α -polarized R spectra means that the main portion of the polarized edge μ -PL, including the disputable $X(\pi)$ line, is from internal regions and is not a characteristic of the outer (near facet) area.

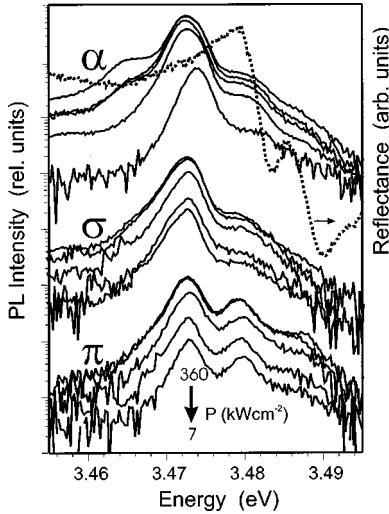


FIG. 5. μ -photoluminescence spectra (solid lines) measured at different excitation power densities in different polarizations. Dotted line presents an α -polarized reflectance spectrum.

B. Power-dependent μ -PL measurements

The spectra measured at different excitation power in three polarizations are presented in Fig. 5. The energy positions of the μ -PL excitonic emission peaks at 4 K in the facet spectra appear to be constant within the range of power densities used, while there is a small low-energy shift of the α -polarized spectrum (Fig. 5). At the level of excitation corresponding to the conventional PL technique ($\sim 10 \text{ W cm}^{-2}$) the near-band-edge PL from the surface (not presented here) appears to be shifted to even higher energy, though the PL still remains within the limits of a reflectance contour. The same dependence on excitation power was observed in II-VI semiconductors.²⁹ The spectra presented demonstrate appreciable saturation of the bound A exciton and the $X(\pi)$ line with increasing power, while the α - and σ -polarized components of the A free exciton, as well as the B exciton, still increase.

The separation between the free and donor bound A excitons in our samples varies in the range of 6.6–6.8 meV, which is consistent with data reported previously.^{8,44,45} To a first approximation we can assume the same binding energy for all three excitons. Since at low temperature the $X(\pi)$ peak has a ~ 6.5 –6.7 meV separation from the B exciton [see Fig. 1(a)], a tentative explanation of the dominant π -polarized line near the A exciton peak could be the mere overlap of the A free with B bound excitons. This may be a result of the particular strain present in our structures. The bound B exciton was previously observed in high-quality homoepitaxial GaN films between the free and donor bound A excitons.^{41,46} The biexcitons having slightly smaller binding energy⁴⁷ of ~ 5.7 meV could also contribute to the μ -PL spectra at high excitation power.

We have performed a decomposition of the polarized spectra by using Lorentzian shape contours, separating for the π -polarization the π -polarized component of the A bound exciton $BX_A(\pi)$, $X(\pi)$, and $FX_B(\pi)$, and for the σ -one— $BX_A(\sigma)$ and $FX_A(\sigma)$. At low temperature $FX_B(\sigma)$ and the C

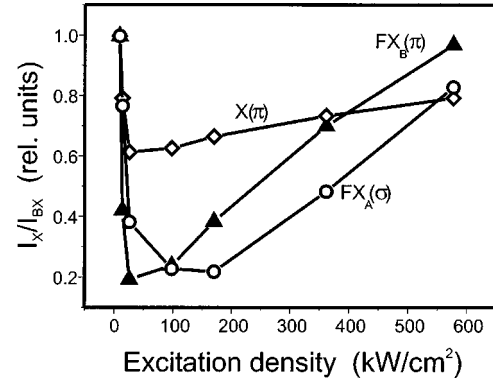


FIG. 6. Relative intensity of polarized μ -PL peaks versus excitation power. The intensities are obtained by division on the intensities of the respectively polarized components of the bound A exciton and normalized to the value at the minimal excitation power. Open diamonds— $X(\pi)$, open circles— $FX_A(\sigma)$, solid triangles— $FX_B(\pi)$.

exciton emissions are negligible. The obtained dependences of integrated intensities on excitation power have also demonstrated some saturation of the $X(\pi)$ line and a full saturation of both polarized components of the bound A exciton. Particularly, the saturation shows a low probability of biexciton formation.

The accuracy of the power measurements is maximal when the relative intensities of the peaks extracted from the same spectrum are compared. Therefore, we present in Fig. 6 the ratio of intensities of the $X(\pi)$, $FX_B(\pi)$, and $FX_A(\sigma)$ components to the respective intensity of either the π - or σ -polarized component of the A bound exciton. For the sake of clarity, the values are normalized to their magnitude at the minimal power. The values drop until the bound exciton emission grows, then, after BX_A saturation, they start to increase. One can see that the relative rise of the $X(\pi)$ peak is much slower than that of both $FX_B(\pi)$ and $FX_A(\sigma)$.

C. Temperature-dependent μ -PL measurements

The temperature variation of the unpolarized μ -PL spectrum measured from a facet [Fig. 7(a)] looks similar to that previously reported for conventional surface PL in high-quality samples.^{40,48,49} The dependence confirms our assignment of the excitonic transitions, e.g., the bound exciton line drops significantly, while the A exciton begins to dominate the spectrum with increasing temperature.

The polarized μ -PL measurements [Fig. 7(b)] provide an unexpected result: the intensity of the $X(\pi)$ peak rises with the temperature increase (when impurity-bound excitons have to be thermally ionized), then drops being resolved up to $T \sim 200$ K. Note that the measurements are done at high enough excitation power density, when all bound states are saturated.

To obtain the energy position and integral intensity of the components, the polarized spectra are decomposed using the following sets of Lorentzian contours: in the π polarization: $BX_A(\pi)$, $X(\pi)$, $FX_B(\pi)$, $FX_C(\pi)$; in the σ polarization: $BX_A(\sigma)$, $FX_A(\sigma)$, and $FX_B(\sigma)$. The last transition, as well

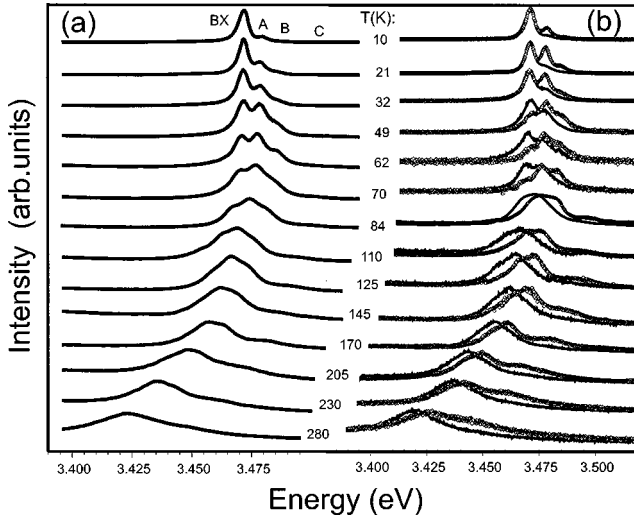


FIG. 7. μ -photoluminescence spectra measured from a facet at different temperatures: (a) unpolarized; (b) π - (open diamonds) and σ - (solid lines) polarized. The spectra are normalized to their maximal peak intensities.

as $\text{FX}_C(\pi)$, is pronounced at temperatures higher than 80 K, while $\text{FX}_C(\sigma)$ is negligible in the whole temperature range. The inset in Fig. 8 illustrates a perfect fitting by an example of the spectra measured at 49 K, when the $X(\pi)$ intensity is almost equal to that of the $\text{FX}_A(\sigma)$. One could assume that the observed strong depolarization in the spectrum near the A exciton is related to an exciton energy increase with increasing temperature, since the selection rules are strongly fulfilled at $\mathbf{k}=0$ only. In this case, the enhancement of differently polarized contributions could be near the free B exciton as well. In contrary, we observed the σ -polarized component near the B exciton to be even smaller than expected for the Γ_5 transition.³⁶

Figure 8 presents the integral intensity variations obtained from the fitting. While the bound exciton is fast and mono-

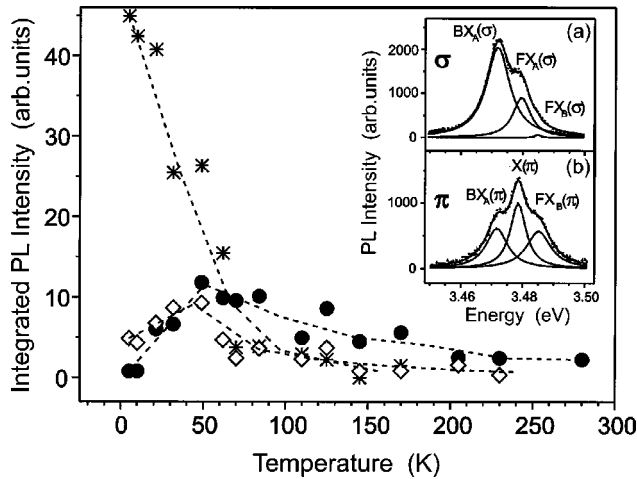


FIG. 8. Integrated intensity of PL polarized components versus temperature: $\text{BX}_A(\sigma)$ —stars, $\text{FX}_A(\sigma)$ —solid circles, and $X(\pi)$ —open diamonds. The inset shows Lorentzian contour decomposition of π - and σ -polarized μ -photoluminescence spectra at 49 K.

tonically weakened, the free-exciton lines first rise with increasing temperature, then decrease slowly. The variation of the $X(\pi)$ intensity is, generally, the same as for the free exciton ones, though with a sharper decrease after 50 K. At higher temperature the remnant part of the $X(\pi)$ is about 1/3 of the $\text{FX}_A(\sigma)$ component.

The temperature variation of polarized μ -PL peak energies obtained as a result of the fitting is presented in Fig. 4(b) together with the C exciton reflectivity data to define the shift in the whole temperature range. To analyze the data we use an analytical four-parameter model proposed by Pässler⁵⁰ and applied recently for successful fitting of data on homoepitaxial GaN.⁴⁸ In the model the temperature variation of band gap is given by

$$E(T) = E(0) - \frac{\alpha_p \Theta_p}{2} \left\{ \frac{\rho}{2} \left[\sqrt{1 + \frac{\pi^2}{6} \left(\frac{4T}{\Theta_p} \right)^2 + \left(\frac{4T}{\Theta_p} \right)^4} - 1 \right] + (1 - \rho) \left[\coth \left(\frac{\Theta_p}{2T} \right) - 1 \right] \right\}, \quad (3)$$

where $E(0)$ is a zero-temperature transition energy; α_p is a high-temperature slope of the dependence; the parameter $0 \leq \rho \leq 1$ determines relative weights of long-wavelength acoustical phonons through linear ρ contribution or a combination of optical and short-wavelength acoustical phonons via singular $(1 - \rho)$; Θ_p is defined via the Debye temperature Θ_D as $\Theta_p \approx 2/3 \Theta_D / (1 - 1/2\rho)$. The weighting parameter ρ has a crucial role in the model, since it allows varying the curvature while both the slope α and point of crossing of high- and low-temperature asymptotes are fixed.

The fit of the μ -PL data has been performed using $E = 3.4810, 3.4858, 3.5053$ eV; $\Theta_p = 420, 400, 420$ K; $\rho = 0.4, 0.3, 0.42$ for $\text{FX}_A(\sigma), \text{FX}_B(\pi), \text{FX}_C(\pi)$, respectively, with the same $\alpha = 0.42$. The fitting of $\text{FX}_B(\pi)$ data by using parameters of $\text{FX}_A(\sigma)$ is obviously worse [dash-dotted line in Fig. 4(b)]. This reflects the nonequidistant spacing of A and B exciton transitions. Previous temperature-dependent studies of GaN performed in the α polarization had frequently shown the nonequidistant spacing ascribed to a different influence of the temperature-induced strain on the A and B exciton energy position (see Ref. 49 and references therein). The strain influence should vary for different crystal orientations. Probably, the difference in ρ values along and normal to the c axis reflects also an anisotropy in phonon spectra in the wurtzite GaN,⁵¹ although it may be related to the difference in group velocities of the respective polariton branches, which also influences phonon-polariton interaction.²⁸ The dependence of $X(\pi)$ energies has a sharper kink as compared to that of the $\text{FX}_A(\sigma)$ at $T \geq 50$ K; so the fitting presented in Fig. 4(b) has been done using the same adjusted parameters as for $\text{FX}_B(\pi)$ with $E = 3.479$ eV.

The fitting of the reflectance data using Eq. (3) shows that the α -polarized R data are generally described by the fitting parameters of the facet μ -PL. The facet reflectivity data are fitted with $E = 3.4780, 3.4830, 3.5053$ eV; $\Theta_p = 100, 200, 420$ K; $\rho = 0.9, 0.85, 0.4$ for $\text{FX}_A(\sigma), \text{FX}_B(\pi), \text{FX}_C(\pi)$, respectively [dashed lines in Fig. 4(a)].

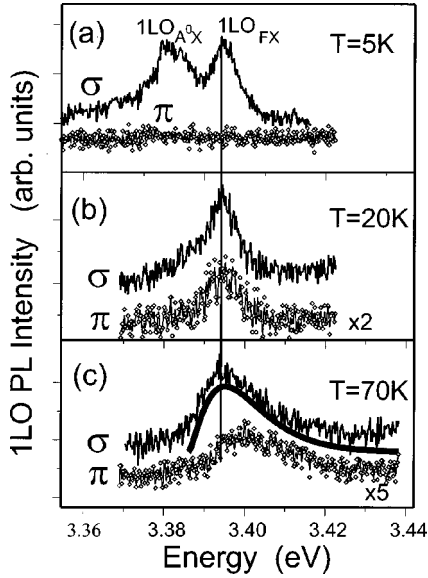


FIG. 9. Spectra of 1LO phonon-assisted emission measured in π - (diamonds) and σ - (thin lines) polarizations at different temperatures: (a) 5 K; (b) 20 K; and (c) 70 K. Solid line, shifted down for clarity in (c), presents the fitting using Maxwell-like distribution.

These strongly varying parameters are hardly meaningful in the model taking into account the phonon interaction only; obviously, anisotropic strain has to be considered to explain the R temperature dependence.

D. Polarized LO phonon-assisted emission

Since the intensity of the no-phonon polariton emission depends on many unknown factors [see Eq. (1)], we performed an analysis of the temperature variation of shape and intensity of the LO phonon-assisted emission, to obtain an information about the real density of states in different polarizations in the vicinity of the A exciton. This emission has to reflect the density of the exciton-polariton states in accordance with Eq. (2), where the probability of exciton recombination $W_m(E)$ is different for the first (1LO) and second (2LO) PL replicas due to different impulse conservation laws for the processes involving one or two phonons.³¹ Assuming a power dependence $W_m(E) \sim E^{l_m}$, where $l_m = 1$ and $l_m = 0$ for the 1LO or 2LO replica, respectively, the energy shift Δ_m between the maximum of the m th replica and its low-energy cutoff should increase linearly with increasing temperature⁵²

$$\Delta_m = (l_m + 1/2)k_B T. \quad (4)$$

The deviation from the law is indicative of defect scattering of exciton-polaritons in GaN or strong thermal nonequilibrium in the crystal lattice.

To confirm the linear law we have used the σ -polarized replicas that appear to be more pronounced compared to the π -polarized replicas at any temperature (Fig. 9). The data presented in Fig. 10(a) concern 1LO replica, since the σ -2LO overlaps partly with a donor acceptor pair (DAP) emission. The experimental shift Δ_i is well consistent with the linear approximation at “high” temperatures (>20 K) and the line shape is well simulated by the $I \sim E^{3/2} \exp(-E/kT)$ depen-

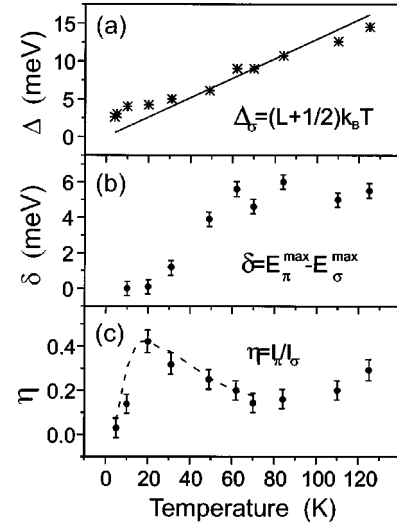


FIG. 10. Temperature dependence of: (a) the shift of the maximum of the σ -polarized 1LO phonon replica from its low-energy cut-off; (b) ratio of intensities of the π - to σ - polarized replicas; and (c) the shift of the maximum of the π -polarized 1LO replica relative to that of σ -1LO.

dence. An example of the 1LO PL shape fitting is shown by solid line in Fig. 9(c) for 70 K. Considering the data at the “high” temperatures, we conclude that the neutral impurity scattering, dominating in the samples studied in Ref. 53 at 50–70 K, is rather small in the top regions of our samples. The observed deviation from the linear law at lower temperature is likely related either to a higher temperature of the crystal lattice, estimated to be ~ 10 K at a nominal temperature of the sample of 5 K, or to polariton scattering by neutral impurities,²⁶ enhanced with decreasing temperature.

At low temperatures (~ 5 K) the intensity of the π -polarized LO PL replicas $I_{\pi LO}$ appears to be negligible compared to the σ -polarized one [Fig. 9(a)]. The $I_{\pi LO}$ value varies in the range $(0-0.1)I_{\sigma LO}$ among the measurements of 20 points on the facets. At the same time, the $X(\pi)$ line exceeds in intensity the σ -polarized A exciton emission at this temperature. This impels us to conclude that the $X(\pi)$ line at 5 K is mostly due to B excitons bound to neutral donors ($D^0 X_B$), whose LO phonon replica may hardly be observed due to a weak LO phonon coupling strength.⁵⁴ On the contrary, 1LO acceptor bound exciton $A^0 X_A$ is well visible in these spectra due to heavier hole masses.

The π -polarized density of occupied states increases noticeably up to 20 K [Fig. 9(b)] in a similar way as the no-phonon free A exciton emission (Fig. 8). The enhancement of the exciton-polariton emission is promoted by temperature-dependent scattering of polaritons inside a branch by longitudinal acoustical (LA) phonons. Within the “high” temperature approximation the probability of the LA phonon scattering of polariton states with wave vector \mathbf{k} increases with increasing temperature as $W^{LA} \sim k(k_B T)$ until disturbance by chaotic thermal vibrations at $T > 100$ K.²⁵ However, the probability is not equal to unity, since polariton states may partly scatter out of the branch, losing their polarization. The process is especially noticeable in the bottle-

neck region, where the σ -polariton undergoes numerous acts of reflections inside the crystal. We believe that the depolarized component might contribute to the $X(\pi)$ line.

The maximum of the π -polarized ILO replica begins to shift after 30 K from the energy position corresponding to the A exciton ILO replica to the B exciton one [Fig. 10(b)]. It looks reasonable, because the π -polarized ILO line should be a superposition of the components related to the scattered A exciton states and the free B exciton. While the former component decreases near 50 K, the latter begins to grow starting from 70 K due to thermally activated occupation of the B exciton band. The ratio of integral intensities of polarized ILO replicas $\eta = I_\pi/I_\sigma$ in the temperature range of 5–60 K can be fitted using an empirical equation

$$\eta = (dI_\sigma/dE_{E-E_0})/T^\nu, \quad (5)$$

where $\nu = 1-1.5$. The good fitting [the dashed line in Fig. 10(c), $\nu = 1.5$] can be obtained if the value of dI_σ/dE is determined in the vicinity of the A exciton energy, namely, within the A exciton linewidth (< 3 meV). This indicates that the effective interbranch scattering between differently polarized exciton-polariton states is effective only with close and small enough polariton wave vectors.

V. DISCUSSION

The above-presented results show that the disputable $X(\pi)$ line really exists in the vicinity of the A exciton and possesses the following controversial characteristics: (i) a low-temperature PL intensity higher than the σ -polarized component of FX_A , (ii) a slow increase (almost saturation) of the intensity with increasing excitation power at low temperatures, (iii) a temperature variation of intensity similar to that for the free excitons. We suppose that only a combined line, whose different constituents dominate at different temperatures, could possess these features. The bound exciton $BX(\Gamma_1)$ and scattered A exciton states including forbidden and mixed ones are probably among its main contributions. We should exclude from the consideration the doublet polariton emission of the B band, due to an energy separation between the π -polarized peaks at least three times larger than Δ_{LT} . Contribution of outer edge B exciton emission (which at low temperature seems to be possible because of the specific band alignment) is not a probable candidate either, since the $X(\pi)$ line follows rather the internal A than the edge B exciton in the whole temperature range studied (Fig. 4).

As for the bound exciton contribution, polaritons can be scattered to excitonlike states and captured by the same scattering impurities that are, presumably, neutral donors in GaN.⁵³ The absence of the π -LO replica at low temperature with intensive $X(\pi)$ confirms the dominance of the D^0X_B contribution, since a LO phonon replica of the B exciton bound on neutral donors should be weak. The contribution appears to be dependent on residual donor concentration like a scattered component observed in Ref. 18. The higher donor concentration in the sample grown on the Si-doped template provides ~ 1.5 increase of the $X(\pi)$ line intensity. The D^0X_B component saturated with increasing excitation power drops

significantly with increasing temperature, because of both exciton delocalization and decrease of polariton scattering efficiency by neutral impurities. For instance, in high-purity InP polariton-impurity interaction is essential up to 30 K only.⁵⁵ Contributions related to the A exciton band can appear at higher temperatures due to increasing exciton-polariton branch population for more effective scattering by LA phonons. Together with imprisonment of the polariton states in the bottleneck region, this results in an increase of the depolarized component. The scattering and mixing of different exciton states at $\mathbf{k} \neq 0$ occur, likely, on defects reducing the crystal symmetry and, hence, lifting of the selection rules.⁵⁶ The existence of real π -polarized states near A exciton in the temperature range of 15–50 K is confirmed by the pronounced π -polarized LO phonon emission shifted exactly on 92 meV from the $X(\pi)$ energy position.

The forbidden exciton $FX_A(\Gamma_6)$ was frequently registered at $\mathbf{k} \perp \mathbf{c}$ in wurtzite compounds,^{5,6,16,24} particularly, due to the strain-induced finiteness of the wave vector. Without external magnetic field this contribution is usually weak in GaN.^{5,6} The lifetime of the forbidden exciton is much longer than that of allowed transitions, which increases the probability to be scattered to the π -polarized polariton branch. Contribution from the mixed states involving the longitudinal polariton $LP(\Gamma_5)$ is possible as well, even at the normal excitation used, as a result of the slight tilt of the c axis. The components might be important at temperatures higher than 50 K.

Thus, the observed temperature and excitation power behavior of the $X(\pi)$ line and temperature variation of the polarized LO phonon-assisted emission permit us to consider this line as a combination of the bound B exciton and several contributions related to the A exciton band. The interplay in intensity between the contributions of different nature, likely, explains the kink in the temperature dependence of the $X(\pi)$ energy. However, there are two disputable items: (i) the bound B exciton originating from Γ_5 states is not directly observed in the spectra; (ii) the PL line related to the free $B(\Gamma_5)$ states is also weak, in spite of the pronounced corresponding feature in the R spectra.

These facts force us to consider the role of polariton kinetics in the enhancement of the $X(\pi)$ line as compared with the $FX_A(\sigma)$ emission. For $\mathbf{k} \perp \mathbf{c}$, different polariton branches coexist in the vicinity of the A exciton with only the polariton branch $LPB_B(\Gamma_1)$ allowed in π polarization [Fig. 2(b)]. The branches differ in their curvature and, hence, in the polariton group velocity ν_p . On one hand, the population and the scattering efficiency of a branch is inversely proportional to ν_p ; on the other hand, the probability of the polaritons to escape from the crystal is directly proportional to the same ν_p value.^{16,57} Near the transverse energy of the B exciton, the group velocity of the $LPB_B(\Gamma_1)$ is low, which permits effective scattering of the exciton-polariton to the π -polarized bound B exciton states. Additional provision can be achieved from the $UPB_B + LPB_C(\Gamma_1)$ branch, whose population is to be enhanced by involving the strong $C(\Gamma_1)$ excitonic states. Thus, the $BX_B(\Gamma_1)$ emission is expected to be strong. At the same time, the combined $UPB_A + LPB_B$ branch [see Fig. 2(b)] permits efficient lowering of the polariton states originating from $B(\Gamma_5)$ to energies corresponding to the A exci-

ton, where the respective emission is assigned as the σ -polarized component of the A exciton. Therefore, the σ -polarized emission in the vicinity of the B exciton can be low. In the vicinity of the A exciton both Γ_5 branches (single LPB_A and combined $\text{UPB}_A + \text{LPB}_B$) are characterized by a low group velocity. This can result in the relatively weak σ -polarized A exciton-polariton emission in this bottleneck. On the contrary, the Γ_1 branch, possessing high ν_p , provides an effective channel for different scattered contributions to emit from the crystal.

It is worth noting that only the joint contributions of the discussed components and peculiarities of the polariton band arrangements at $\mathbf{k} \perp \mathbf{c}$ can result in the observed $X(\pi)$ enhancement and its temperature behavior. We believe that a final decision about the preferable mechanism needs additional studies, e.g., time-resolved and magneto-optical μ -PL measurements may be especially useful.

VI. CONCLUSIONS

We have studied polarized μ -PL of thick GaN layers and demonstrated an enhanced π -polarized PL line in the vicinity of the A exciton. The line originates mostly from the internal body of the layers and exceeds in intensity the σ -polarized A exciton at low temperature. A complex nature of the emission is suggested to explain the observed specific temperature- and power-dependent behavior of the π -polarized PL line. The analysis of polarized LO phonon-

assisted emission has shown that the bound B exciton appears to be an essential component of the line at low temperatures, while contributions from scattered A exciton states become appreciable when the temperature rises. The enhancement of the π -polarized PL components can be enforced by the high group velocity of the $B(\Gamma_1)$ branch in the vicinity of the A exciton, which provides an effective channel for PL emission from the crystal.

The μ -PL and R studies reveal also inequalities in optical properties of cleaved edge and top surface regions in the GaN layers, tentatively explained as induced by a different strain in these regions. The observed band alignment in outer and internal regions is important for the edge-emitting devices, such as LED and lasers, since the absorption edge of the material adjusting to the cleaved edges appears to be below the energy of emission from internal regions, which can induce additional losses.

ACKNOWLEDGMENTS

This work was partly supported by the Program of the Ministry of Sciences of RF “Physics of Solid State Nanostructures” and RFBR Grants Nos. 99-02-17103 and 00-02-17022. The work at Linköping University was partly supported by the European Community via the CLERMONT project HPRN-CT-1999-00132. The authors thank Professor E.L. Ivchenko for fruitful discussions and Dr. E.S. Moskalenko for expert assistance in μ -PL measurements.

-
- ¹R. Dingle, D. D. Sell, S. E. Stokowski, and M. Ilegems, *Phys. Rev. B* **4**, 1211 (1971).
- ²J. J. Hopfield, *J. Phys. Chem. Solids* **15**, 97 (1960).
- ³S. Chichibu, T. Azuhata, T. Sota, H. Amano, and I. Akasaki, *Appl. Phys. Lett.* **70**, 2085 (1997).
- ⁴L. Eckey, L. Podlowski, A. Göldner, A. Hoffmann, I. Broser, B. K. Meyer, D. Volm, T. Streibl, K. Hiramatsu, T. Detchprohm, H. Amano, and I. Akasaki, *Inst. Phys. Conf. Ser.* **142**, 943 (1996).
- ⁵L. Eckey, A. Hoffmann, P. Thurian, I. Broser, B. K. Meyer, and K. Hiramatsu, in *Nitride Semiconductors*, edited by F. A. Ponce, S. P. DenBaars, B. K. Meyer, S. Nakamura, and S. Strite, *Mater. Res. Soc. Symp. Proc. No. 482* (Materials Research Society, Pittsburgh, 1998), p. 555.
- ⁶D. C. Reynolds, D. C. Look, B. Jogai, A. W. Saxler, S. S. Park, and J. Y. Hahn, *Appl. Phys. Lett.* **77**, 2879 (2000).
- ⁷H. Siegle, A. Hoffmann, L. Eckey, C. Thomsen, J. Christen, F. Bertram, D. Schmidt, D. Rudloff, and K. Hiramatsu, *Appl. Phys. Lett.* **71**, 2490 (1997).
- ⁸B. Monemar, *Phys. Rev. B* **10**, 676 (1974).
- ⁹B. Gil, O. Briot, and R. L. Aulombard, *Phys. Rev. B* **52**, R17 028 (1995).
- ¹⁰J. Liu, N. R. Perkins, M. N. Horton, J. M. Redwing, M. A. Tischler, and T. F. Kuech, *Appl. Phys. Lett.* **69**, 3519 (1996).
- ¹¹X. Li, P. W. Bohn, and J. J. Coleman, *Appl. Phys. Lett.* **75**, 4049 (1999).
- ¹²A. Vertikov, M. Kuball, A. V. Nurmikko, Y. Chen, and S.-Y. Wang, *Appl. Phys. Lett.* **72**, 2645 (1998).
- ¹³W. D. Herzog, R. Singh, T. D. Moustakas, B. B. Goldberg, and M. S. Ünlü, *Appl. Phys. Lett.* **70**, 1333 (1997).
- ¹⁴T. V. Shubina, A. A. Toropov, V. V. Ratnikov, R. N. Kyutt, S. V. Ivanov, T. Paskova, E. Valcheva, and B. Monemar, *IPAP Conf. Series 1: IWN2000*, p. 595 (2000).
- ¹⁵E. L. Ivchenko and G. E. Pikus, in *Superlattices and Other Heterostructures*, edited by M. Cardona, P. Flude, K. von Klitzing, and H.-J. Queisser, *Springer Series in Solid-State Sciences* (Springer, New York, 1997), Vol. 110, Chap. 5.
- ¹⁶J. J. Hopfield, *Phys. Rev.* **112**, 1555 (1958).
- ¹⁷C. Weisbuch and R. G. Ulbrich, *J. Lumin.* **18/19**, 27 (1979).
- ¹⁸R. Stepniowski, K. P. Korona, A. Wyszniak, J. M. Baranowski, K. Pakula, M. Potemski, G. Martinez, I. Grzegory, and S. Porowski, *Phys. Rev. B* **56**, 15 151 (1997).
- ¹⁹K. Kornitzer, T. Ebner, M. Grehl, K. Thonke, R. Sauer, C. Kirchner, V. Schwegler, M. Kamp, M. Leszczynski, I. Grzegory, and S. Porowski, *Phys. Status Solidi B* **216**, 5 (1999).
- ²⁰K. Torii, T. Deguchi, T. Sota, K. Suzuki, S. Chichibu, and S. Nakamura, *Phys. Rev. B* **60**, 4723 (1999).
- ²¹S. F. Chichibu, K. Torii, T. Deguchi, T. Sota, A. Setoguchi, H. Nakanishi, T. Azuhata, and S. Nakamura, *Appl. Phys. Lett.* **76**, 1576 (2000).
- ²²F. Bertram, S. Srinivasan, F. A. Ponce, T. Riemann, J. Christen, and R. J. Molnar, *Appl. Phys. Lett.* **78**, 1222 (2001).
- ²³T. Paskova, S. Tungasmita, E. Valcheva, E. Svedberg, B. Arnau-dov, S. Evtimova, P. O. A. Persson, A. Henry, R. Beccard, M. Heuken, and B. Monemar, *MRS Internet J. Nitride Semicond. Res.* **5S1**, W3.14 (2000).

- ²⁴C. Benoit à la Guillaume, A. Bonnot, and J. M. Debever, *Phys. Rev. Lett.* **24**, 1235 (1970).
- ²⁵W. C. Tait and L. Weiner, *Phys. Rev.* **166**, 769 (1968).
- ²⁶E. S. Koteles, J. Lee, J. P. Salerno, and M. O. Vassell, *Phys. Rev. Lett.* **55**, 867 (1985).
- ²⁷W. S. Tait and R. L. Weiher, *Phys. Rev.* **178**, 1404 (1969).
- ²⁸Y. Toyozawa, *Prog. Theor. Phys. Suppl.* **12**, 111 (1959).
- ²⁹E. F. Gross, S. A. Permagorov, V. V. Travnikov, A. V. Sel'kin, *Fiz. Tverd. Tela (Leningrad)* **13**, 699 (1971) [*Sov. Phys. Solid State* **13**, 699 (1971)].
- ³⁰B. Gil, S. Clur, and O. Briot, *Solid State Commun.* **104**, 267 (1997).
- ³¹E. F. Gross, S. A. Permagorov, and B. S. Razbirin, *Usp. Fiz. Nauk* **14**, 104 (1971) [*Sov. Phys.-Usp.* **14**, 104 (1971)].
- ³²S. A. Permagorov, in *Physics of II-VI Compounds*, edited by A. N. Georgobiani and M. K. Shakeman (Nauka, Moscow, 1986), p. 146.
- ³³B. Gil and O. Briot, *Phys. Rev. B* **55**, 2530 (1997).
- ³⁴M. Susaki, K. Wakita, and N. Yamamoto, *Jpn. J. Appl. Phys., Part 1* **38**, 2787 (1999).
- ³⁵V. Ratnikov, R. Kyutt, T. Shubina, T. Paskova, E. Valcheva, and B. Monemar, *J. Appl. Phys.* **88**, 6252 (2000).
- ³⁶B. Gil, in *Gallium Nitride II*, edited by J. I. Pankove and T. D. Moustakas (Academic, New York, 1999), Vol. 57, p. 209.
- ³⁷K. Kornitzer, T. Ebner, K. Thonke, R. Sauer, C. Kirchner, V. Schwegler, M. Kamp, M. Leszczynski, I. Grzegory, and S. Porowski, *Phys. Rev. B* **60**, 1471 (1999).
- ³⁸V. V. Krivolapchuk, S. A. Permagorov, and V. V. Travnikov, *Fiz. Tverd. Tela (USA)* **23**, 343 (1981) [*Sov. Phys.-Solid State* **23**, 606 (1981)]; V. V. Travnikov and V. V. Krivolapchuk, *Pis'ma Zh. Eksp. Teor. Fiz.* **34**, 347 (1981) [*Sov. Phys.-Solid State* **34**, 347 (1981)].
- ³⁹V. V. Travnikov and V. V. Krivolapchuk, *Pis'ma Zh. Eksp. Teor. Fiz.* **37**, 419 (1983) [*JETP Lett.* **37**, 496 (1983)].
- ⁴⁰B. Monemar, J. P. Bergman, I. A. Buyanova, W. Li., H. Amano, and I. Akasaki, *MRS Internet Nitride Semicond. Res.* **1**, 2 (1997).
- ⁴¹K. Kornitzer, M. Grehl, K. Thonke, R. Sauer, C. Kirchner, V. Schwegler, M. Kamp, M. Leszczynski, I. Grzegory, and S. Porowski, *Physica B* **273-274**, 66 (1999).
- ⁴²J. J. Hopfield and D. J. Thomas, *Phys. Rev.* **132**, 563 (1963).
- ⁴³K. Domen, H. Horino, A. Karamata, and T. Tanahashi, *Appl. Phys. Lett.* **70**, 987 (1997).
- ⁴⁴K. Naniwae, S. Itoh, H. Amano, K. Itoh, K. Hiramatsu, and I. Akasaki, *J. Cryst. Growth* **99**, 381 (1990).
- ⁴⁵A. Viswanath, J. I. Lee, S. Yu. D. Kim, Y. Choi, and C.-H. Hong, *J. Appl. Phys.* **84**, 3848 (1998).
- ⁴⁶A. Wyszomolek, V. F. Sapega, T. Ruf, M. Cardona, M. Potemski, P. Wyder, R. Stepniewski, K. Pakula, J. M. Baranowski, I. Grzegory, and S. Porowski, *IPAP Conf. Series 1: IWN2000*, p. 579 (2000).
- ⁴⁷Y. Kawakami, Z. G. Peng, Y. Narukawa, Sz. Fujita, Sg. Fujita, and S. Nakamura, *Appl. Phys. Lett.* **69**, 1414 (1996).
- ⁴⁸K. Thonke, K. Kornitzer, M. Grehl, R. Sauer, C. Kirchner, V. Schwegler, M. Kamp, M. Leszczynski, I. Grzegory, and S. Porowski, *IPAP Conf. Series 1: IWN2000*, p. 587 (2000).
- ⁴⁹L. Siozade, S. Colard, M. Mihailovic, J. Leymarie, A. Vasson, N. Grandjean, M. Leroux, and J. Massies, *Jpn. J. Appl. Phys., Part 1* **39**, 20 (2000).
- ⁵⁰R. Pässler, *J. Appl. Phys.* **83**, 3356 (1998).
- ⁵¹K. Torii, M. Ono, T. Sota, T. Azuhata, S. F. Chichibu, and S. Nakamura, *Phys. Rev. B* **62**, 10 861 (2000).
- ⁵²S. A. Permagorov, in *Excitons*, edited by E. I. Rashba and M. D. Sturge (North-Holland Amsterdam, 1982), p. 177.
- ⁵³I. A. Buyanova, J. P. Bergman, B. Monemar, H. Amano, I. Akasaki, A. Wyszomolek, P. Lomiak, J. M. Baranowski, K. Pakula, R. Stepniewski, K. P. Korona, I. Grzegory, M. Bockowski, and S. Porowski, *Solid State Commun.* **8**, 497 (1998).
- ⁵⁴J. Jayapalan, B. J. Skromme, R. P. Vaudo, and V. M. Phanse, *Appl. Phys. Lett.* **73**, 1188 (1998).
- ⁵⁵R. Benzaquen, R. Leonelli, and S. Charbonneau, *Phys. Rev. B* **59**, 1973 (1999).
- ⁵⁶H. M. Cheong, Y. Zhang, A. Mascarenhas, J. F. Geisz, and J. M. Olson, *Appl. Phys. Lett.* **83**, 1773 (1998).
- ⁵⁷E. L. Ivchenko, A. B. Selkin, A. G. Abdukadyrov, M. I. Sazhin, and N. H. Uldashev, *Opt. Spektrosk.* **67**, 296 (1989) [*Opt. Spectrosc.* **67**, 496 (1989)].